Ab initio calculations on SF_2 and its low-lying cationic states: Anharmonic Franck-Condon simulation of the uv photoelectron spectrum of SF_2

Edmond P. F. Lee,[a),b)] Daniel K. W. Mok,[a),c)] and Foo-tim Chau
Department of Applied Biology and Chemical Technology, Hong Kong Polytechnic University, Hung Hom, Hong Kong

John M. Dyke
School of Chemistry, University of Southampton, Highfield, Southampton SO17 1BJ, United Kingdom

(Received 17 January 2006; accepted 21 June 2006; published online 8 September 2006)

Geometry optimization calculations were carried out on the $\tilde{X}\,^1A_1$ state of SF_2 and the $\tilde{X}\,^2B_1$, $\tilde{A}\,^2A_1$, $\tilde{B}\,^2B_2$, $\tilde{C}\,^2B_2$, $\tilde{D}\,^2A_1$, and $\tilde{E}\,^2A_2$ states of SF_2^+ employing the restricted-spin coupled-cluster single-double plus perturbative triple excitation [RCCSD(T)] method and basis sets of up to the augmented correlation-consistent polarized quintuple-zeta [aug-cc-pV(5+*d*)Z] quality. Effects of core electron (S $2s^22p^6$ and F $1s^2$ electrons) correlation and basis set extension to the complete basis set limit on the computed minimum-energy geometries and relative electronic energies (adiabatic and vertical ionization energies) were investigated. RCCSD(T) potential energy functions (PEFs) were calculated for the $\tilde{X}\,^1A_1$ state of SF_2 and the low-lying states of SF_2^+ listed above employing the aug-cc-pV(5+*d*)Z and aug-cc-pV5Z basis sets for S and F, respectively. Anharmonic vibrational wave functions of these neutral and cationic states of SF_2, and Franck-Condon (FC) factors of the lowest four one-electron allowed neutral photoionizations were computed employing the RCCSD(T) PEFs. Calculated FC factors with allowance for Duschinsky rotation and anharmonicity were used to simulate the first four photoelectron bands of SF_2. The agreement between the simulated and observed first bands in the He I photoelectron spectrum reported by de Leeuw *et al.* [Chem. Phys. **34**, 287 (1978)] is excellent. Our calculations largely support assignments made by de Leeuw *et al.* on the higher ionization energy bands of SF_2. © *2006 American Institute of Physics*. [DOI: 10.1063/1.2227380]

INTRODUCTION

SF_2 has received considerable attention in the past from both spectroscopists and computational chemists partly because of its importance in the semiconductor industry, for example, as a reactive intermediate in plasma etching by SF_6/O_2 plasmas (see Ref. 1 and references therein). In this connection, the ground and a large number of excited electronic states (from the $\tilde{A}$ state to the $\tilde{J}$ state) of SF_2 have been characterized by spectroscopic[2–10] and/or computational[1,10–16] means. Since a fairly comprehensive description of previous experimental and theoretical studies of SF_2 has been given in the Introduction of a very recent computational study by the *R*-matrix method on electron collisions with SF_2, readers are referred to Ref. 1 (and references therein) for details of previous work on SF_2. When compared with the neutral molecule, SF_2^+ has, however, received significantly less attention. Nevertheless, the first adiabatic ionization energy (AIE) of SF_2 has been measured or derived from electron-impact mass-spectrometric,[17,18] photoionization mass-spectrometric,[19] photoelectron[20] (PE), and resonance-enhanced multiphoton ionization[7] (REMPI) studies. In addition, the first AIE of SF_2 has been computed at the G2 level of theory in two separate computational studies, both focusing on the thermochemistry of SF_n series (from $n=1$ up to $n=6$) and their ions[21,22] in relation to plasma chemistry. For the low-lying excited cationic states of SF_2^+, the only experimental study available is the He I PE spectrum, which was reported by de Leeuw *et al.*[20] over 25 years ago. The observed PE spectrum clearly shows the first band with well resolved vibrational structure. However, the higher ionization energy (IE) bands of SF_2 are heavily overlapped with PE bands of other species (such as HF, SF_4, SF_6, and also some unidentifiable species; see Ref. 20 for details), and no vibrational structure associated with any excited cationic states of SF_2^+ could be observed in the higher IE bands observed in the He I PE spectrum.[20] Nevertheless, with the aid of computed vertical ionization energies (VIEs) obtained from semiempirical (negative of CNDO/2 and CNDO/S eigenvalues reduced by 20%), Hartree-Fock-Slater (HFS) (VIEs calculated by the transition state method), and earlier *ab initio* (HF/[4*s*3*p*1*d*],[2*s*1*p*]; 92% of Koopman's theorem)[23] calculations, ionizations to five excited cationic states of SF_2^+ were assigned to spectral features observed in the higher IE region of the He I PE spectrum reported in Ref. 20. Since then, there has been no further investigation on excited cationic states of SF_2^+ to our knowledge. In view of the relatively low level of theory used to calculate the VIEs

[a)]Authors to whom correspondence should be addressed.
[b)]Also at University of Southampton, Highfield, Southampton SO17 1BJ, UK. Electronic mail: epl@soton.ac.uk
[c)]Electronic mail: bcdaniel@polyu.edu.hk

of the low-lying excited states of SF_2^+ in previous studies,[20,23] it is proposed in the present study to carry out state-of-the-art *ab initio* calculations on the low-lying cationic state of SF_2^+ and also to simulate the He I PE spectrum of SF_2 employing our combined *ab initio*/Franck-Condon (FC) method including anharmonicity.[24–26]

THEORETICAL CONSIDERATIONS AND COMPUTATIONAL DETAILS

Ab initio calculations

Geometry optimizations on the $\tilde{X}\,^1A_1$ state of SF_2 and the $\tilde{X}\,^2B_1$, $\tilde{A}\,^2A_1$, $\tilde{B}\,^2B_2$, $\tilde{C}\,^2B_2$, $\tilde{D}\,^2A_1$, and $\tilde{E}\,^2A_2$ states of SF_2^+ were carried out employing the restricted-spin coupled-cluster single and double plus perturbative triple excitation [RCCSD(T)] method.[27,28] Two different combinations of basis sets of valence quadruple-zeta and quintuple-zeta qualities, namely, the aug-cc-pV(Q+*d*)Z/aug-cc-pVQZ and aug-cc-pV(5+*d*)Z/aug-cc-pVQZ basis sets,[29] were used for S/F. With these basis sets, the frozen core approximation was applied in the RCCSD(T) calculations. Nevertheless, effects of core electron correlation on computed minimum-energy geometries and relative electronic energies (AIEs and VIEs) were investigated using core-valence basis sets of quadruple-zeta quality, namely, the aug-cc-pwCVQZ/aug-cc-pCVQZ basis sets[30] for S/F. With these core-valence basis sets, only the S $1s^2$ electrons were frozen in the RCCSD(T) calculations, i.e., the S $2s^22p^6$ and F $1s^2$ electrons were included in the correlation calculations in addition to valence electrons.

Contributions of basis set extension to the complete basis set (CBS) limit to the computed AIE/VIE values were estimated by taking half of the differences between the corresponding values obtained using the valence quintuple-zeta and quadruple-zeta quality basis sets (see Ref. 31 for the theoretical basis of this simple method of basis set extrapolation). Contributions of core electron correlation to the computed AIE/VIE values were estimated by taking the differences of the corresponding values obtained using the core-valence quadruple-zeta basis sets [including the S $2s^22p^6$ and F $1s^2$ electrons in the RCCSD(T) calculations] and the valence quadruple-zeta basis sets (within the frozen core approximation). The contributions of basis size extension and core electron correlation to the computed relative electronic energies have been assumed to be additive.

Relativistic effects on the computed AIE values have also been investigated. Relativistic contributions were calculated by two different methods as implemented in the MOLPRO suite of programs.[32] First, the expectation values of the mass-velocity and Darwin terms were calculated employing the Cowan-Griffin operator with the Hartree-Fock wave function. Second, relativistic self-consistent-field (SCF) calculations were carried out employing the Douglas-Kroll relativistic one-electron integrals. In this case, the relativistic contribution was taken as the difference between the total energies obtained from the relativistic SCF calculation and the nonrelativistic Hartree-Fock calculation $[E_{\mathrm{rel}}(\mathrm{DK})-E_{\mathrm{nonrel}}(\mathrm{HF})]$ employing the same basis set. The uncontracted aug-cc-pVQZ basis set was used in these relativistic calculations. From previous experience, this basis set should be adequate.[31,33] Also, similar to previous findings,[31,33] the results obtained employing the above-mentioned two methods are essentially identical and hence only one set of the results are present below.

Some additional single energy complete active space SCF (CASSCF)/multireference configuration interaction (MRCI) calculations[34,35] were carried out on the $\tilde{X}\,^1A_1$ state of SF_2 and the two lowest doublet cationic states of each of the A_1, B_1, B_2, and A_2 symmetries of the C_{2v} point group. The aug-cc-pV(Q+*d*)Z/aug-cc-pVQZ basis sets for S/F were used and the CASSCF/MRCI calculations were performed at the RCCSD(T) optimized geometry of the $\tilde{X}\,^1A_1$ state of SF_2 using the same basis sets. A full valence active space was employed, and in the averaged-state CASSCF calculations, equal weights for the two lowest doublet states of each symmetry were requested. The subsequent two-state MRCI calculations for each symmetry generated up to 1.018×10^9 uncontracted configurations and 4.173×10^6 internally contracted configurations. These CASSCF/MRCI calculations give the VIEs to eight low-lying cationic states of SF_2^+ and hence the relative electronic energies of these cationic states in the FC region.

RCCSD(T) energy scans employing the aug-cc-pV(5+*d*)Z/aug-cc-pV5Z basis sets for S/F were carried out on the $\tilde{X}\,^1A_1$ state of SF_2 and the $\tilde{X}\,^2B_1$, $\tilde{A}\,^2A_1$, $\tilde{B}\,^2B_2$, $\tilde{C}\,^2B_2$, $\tilde{D}\,^2A_1$, and $\tilde{E}\,^2A_2$ states of SF_2^+. The ranges of bond lengths and angles and the number of energy points used in these energy scans are given in Table I (energy scans were only carried out in the symmetric stretching and bending coordinates; see the next subsection). Within these ranges of energy scans, the computed values of the T_1 diagnostic are small, indicating that multireference character is not important for these energy points. These energy points were used for the fitting of the potential energy function (PEF) of each electronic state considered (see the next subsection).

TABLE I. The ranges of bond lengths [r(SF) in Å] and bond angles [θ(FSF) in deg], the number of points employed in the RCCSD(T)/aug-cc-pV(5+*d*)Z, aug-cc-pV5Z (for S,F) energy scans, which were used for the fitting of the potential energy functions (PEFs) of the different electronic states of SF_2 and its cation, the maximum vibrational quantum numbers of the symmetric stretching (v_1) and bending (v_2) modes of the harmonic basis used in the variational calculations of the anharmonic vibrational wave functions of each electronic state, and the restrictions of the maximum values of (v_1+v_2).

States	Range of r(SF)	Range of θ(FSF)	Points	Max. v_1	Max. v_2	Max. (v_1+v_2)
$\tilde{X}\,^1A_1$	1.1–2.5	60–150	100	10	10	10
$\tilde{X}\,^2B_1$	0.9–2.5	60–165	148	20	20	20
$\tilde{A}\,^2A_1$	1.3–1.8	73–179	95	[a]	[a]	[a]
$\tilde{B}\,^2B_2$	1.04–1.78	65–138	80	5	8	8
$\tilde{C}\,^2B_2$	1.25–2.5	45–132	129	35	50	50
$\tilde{D}\,^2A_1$	0.97–2.1	64–167	116	20	20	20
$\tilde{E}\,^2A_2$	1.3–2.15	60–139	119	20	25	25

[a]The bending mode is very anharmonic and the results of the variational calculation on the $\tilde{A}\,^2A_1$ state are very dependent on the harmonic basis used; see also footnote d of Table IV.

In addition to computed vibrational frequencies obtained from variational calculations to be described (see the next subsection) employing the *ab initio* PEFs just discussed, harmonic vibrational frequencies were also calculated numerically for the $\tilde{X}\,^1A_1$ state of SF_2 and the $\tilde{X}\,^2B_1$ state of SF_2^+ at their respective equilibrium geometries. These harmonic frequency calculations were carried out at the RCCSD(T) level with the valence quadruple-zeta quality basis sets and they gave harmonic frequencies of all three vibrational modes (i.e., including the asymmetric stretching mode; variational calculations of anharmonic vibrational wave functions employing *ab initio* PEFs to be discussed have considered only the symmetric stretching and bending modes; see the next subsection). Zero-point energy correction (ΔZPE) for the first AIE of SF_2 (i.e., ionization leading to the $\tilde{X}\,^2B_1$ state of SF_2^+) has been made using the computed harmonic vibrational frequencies of all three modes. ΔZPEs for higher AIEs, however, have been evaluated using only the computed fundamental frequencies of the symmetric stretching and bending modes obtained from the variational calculations using the *ab initio* PEFs. Based on computed vibrational frequencies of all three modes for the $\tilde{X}\,^1A_1$ state of SF_2 and the $\tilde{X}\,^2B_1$ state of SF_2^+, the difference between including and excluding the asymmetric stretching mode in the evaluation of ΔZPE for the first AIE of SF_2 is −0.011 eV. In this connection, it seems reasonable to assume that the uncertainties associated with the neglect of the asymmetric stretching mode in the evaluation of ΔZPE for higher IE bands are of the order of ±0.01 eV, and this has been included in the estimated uncertainties associated with the computed AIE_0 values of the higher IE bands.

All *ab initio* calculations reported here were carried out using MOLPRO.[32]

Potential energy functions, anharmonic vibrational wave functions, and Franck-Condon factor calculations

For each electronic state studied, the potential energy function V was determined by fitting the following polynomial to an appropriate number of single point energies as discussed above:

$$V = \sum_{ij} C_{ij}(S_1)^i(S_2)^j + V_{\mathrm{eqm}}. \tag{1}$$

S_1 (the symmetric stretching) in the PEF is expressed in terms of a Morse-type coordinate,[36]

$$S_1 = [1 - e^{-\gamma(r-r_{\mathrm{eqm}})/r_{\mathrm{eqm}}}]/\gamma, \tag{2}$$

where r is the SF bond length and r_{eqm} is the equilibrium bond length. S_2 (the symmetric bending) is expressed as

$$S_2 = \Delta\theta + \alpha(\Delta\theta^2) + \beta(\Delta\theta)^3, \tag{3}$$

where $\Delta\theta$ is the displacement in the θ(FSF) bond angle from the corresponding equilibrium value.[37] The nonlinear least squares fitting procedure,[38] NL2SOL, was employed to obtain the C_{ij}, V_{eqm}, r_{eqm}, θ_{eqm}, α, β, and γ values from the computed single point energy data. The asymmetric stretching mode has not been considered, because the observed first band in the He I PE spectrum of Ref. 20 with resolved vibrational structure does not show any identifiable vibrational structure associated with the asymmetric stretching mode, and for ionization from a C_{2v} molecule to a C_{2v} cation, this mode is only allowed in double quantum excitations.

Variational calculations, which employed the rovibronic Hamiltonian of Watson for a nonlinear molecule[39] and the *ab initio* PEFs discussed above, were carried out to obtain the anharmonic vibrational wave functions and their corresponding energies (see Refs. 24 and 25 for details). The anharmonic vibrational wave functions were expressed as linear combinations of harmonic oscillator functions, $h(v_1,v_2)$, where v_1 and v_2 denote the quantum numbers of the harmonic basis functions for the symmetric stretching and bending modes, respectively.[24,25] The maximum v_1 and v_2 values of the harmonic basis used and the restriction of the maximum magnitude of (v_1+v_2) imposed for each electronic state studied are given in Table I. Franck-Condon factors were computed employing the anharmonic vibrational wave functions and allowing for Duschinsky rotation, as described previously.[25,26]

Four PE bands, which lead to the $\tilde{X}\,^2B_1$, $\tilde{C}\,^2B_2$, $\tilde{D}\,^2A_1$, and $\tilde{E}\,^2A_2$ states of SF_2^+ via one-electron allowed ionization processes, have been simulated. The relative intensity of each vibrational component in a simulated PE band is given by the corresponding computed anharmonic FC factor.

RESULTS AND DISCUSSIONS

The coefficients of the fitted polynomials, C_{ij} [in Eq. (1)], the values of γ and α [in Eqs. (2) and (3), respectively], and the root-mean-square (rms) deviations of the fitted PEFs from the *ab initio* data points for the $\tilde{X}\,^1A_1$ state of SF_2 and the $\tilde{X}\,^2B_1$, $\tilde{C}\,^2B_2$, $\tilde{D}\,^2A_1$, and $\tilde{E}\,^2A_2$ states of SF_2^+ are given in Table II. *Ab initio* results obtained in the present study are summarized in Tables III–VI together with available experimental and theoretical values for comparison. Simulated PE bands of SF_2 are presented in Figs. 1–5.

Before results from *ab initio* calculations are discussed, it should be noted that the $\tilde{X}\,^1A_1$ state of SF_2 has the electronic configuration of $\cdots(8a_1)^2(3b_1)^2(5b_2)^2(1a_2)^2$. Our calculations show that the lowest $^2A_1$ and $^2B_2$ states, i.e., the $(1)^2A_1$ and $(1)^2B_2$ states, of SF_2^+ have the electronic configurations of $\cdots(9a_1)^1(2b_1)^2(5b_2)^2(1a_2)^2$ and $\cdots(8a_1)^2(2b_1)^2(6b_2)^1(1a_2)^2$, respectively. In order to reach these two cationic states from the $\tilde{X}\,^1A_1$ state of SF_2, both ionization of an electron from the $3b_1$ molecular orbital and excitation of an electron from the $3b_1$ molecular orbital to the $9a_1$ or $6b_2$ molecular orbital, respectively, are required. These two cationic states cannot be reached via a one-electron ionization process from the $\tilde{X}\,^1A_1$ state of SF_2 and hence ionizations to these states are formally forbidden. However, because their minima have computed electronic energies between those of the $\tilde{X}\,^2B_1$ and $\tilde{C}\,^2B_2$ states of SF_2^+ (hence they are the $\tilde{A}\,^2A_1$ and $\tilde{B}\,^2B_2$ states of SF_2^+), their

TABLE II. RCCSD(T)/aug-cc-pV(5+*d*)Z,aug-cc-pV5Z for (S,F) potential energy functions (PEFs) of the $\tilde{X}\,^1A_1$ state of SF_2 and the $\tilde{X}\,^2B_1$, $\tilde{C}\,^2B_1$, $\tilde{D}\,^2A_1$, and $\tilde{E}\,^2A_2$ states of SF_2^+ (C_{ij} are the coefficients of the polynomials used for the PEFs [Eq. (1)]).

C_{ij}	$\tilde{X}\,^1A_1$	$\tilde{X}\,^2B_1$	$\tilde{C}\,^2B_2$	$\tilde{D}\,^2A_1$	$\tilde{E}\,^2A_2$
C_{20}	3.064 128 9	3.861 930 2	2.703 806 8	2.442 018 6	2.323 342 4
C_{11}	0.056 413 5	0.117 021 1	0.523 924 5	0.079 044 3	0.080 653 7
C_{02}	0.146 869 0	0.170 001 6	0.272 359 0	0.068 515 4	0.116 477 7
C_{30}	−5.741 539 4	−6.964 687 3	−3.303 669 0	−0.906 148 0	−5.784 497 4
C_{21}	−0.482 166 0	−0.640 051 6	−2.107 908 3	0.099 050 6	−0.642 202 9
C_{12}	−0.589 455 8	−0.650 551 7	−2.170 433 5	−0.363 358 4	−0.693 232 9
C_{03}	−0.022 221 9	−0.013 840 6	−0.476 911 9	0.001 345 9	−0.078 614 3
C_{40}	6.189 245 8	6.836 454 4	0.833 920 1	1.387 504 5	8.219 068 0
C_{22}	1.088 844 9	1.037 702 0	4.211 888 4	−0.128 240 7	2.105 500 3
C_{04}	0.086 728 2	0.086 100 1	0.659 229 4	0.014 607 4	0.139 468 1
C_{31}	0.286 058 4	0.310 561 9	2.682 386 1	−0.007 888 5	0.684 519 8
C_{13}	1.390 692 2	1.569 782 9	1.939 528 2	−0.759 404 1	2.169 247 9
C_{05}	−0.026 280 7	−0.032 404 6	−0.526 550 8	−0.051 954 3	−0.115 774 2
C_{06}	0.050 180 9	0.074 931 2	0.244 905 9	0.059 545 5	0.083 490 9
C_{50}	−7.324 207 6	−8.874 518 3	3.934 218 5	17.498 255	−12.241 651
C_{60}	2.455 983 2	−2.742 273 7	23.267 359	57.245 830	15.695 879
C_{41}	−1.316 113 1	−0.993 537 4	0.077 859 4	−2.022 784 9	−4.024 279 4
C_{32}	−1.517 653 5	−1.133 573 2	−0.284 033 6	1.147 584 4	−3.556 190 2
C_{23}	−1.050 301 6	−1.057 989 4	−2.420 111 5	−0.778 891 8	−2.199 815 0
C_{14}	−0.476 308 9	−0.422 826 4	−2.230 242 3	−0.100 938 4	−0.908 689 0
C_{51}	0.022 866 0	0.040 390 7	0.252 747 6	0.116 079 0	−0.026 053 9
C_{42}	0.024 947 7	0.008 548 8	−0.221 075 6	0.067 924 2	0.019 853 8
C_{33}	−1.321 786 2	3.982 544 5	−70.905 935	93.120 312	−9.859 593 2
C_{24}	4.222 843 7	12.399 345	−259.405 32	56.558 954	0.166 629 4
C_{15}	0.096 043 1	−1.242 636 4	−4.296 177 9	−0.569 926 0	2.107 188 2
C_{07}	1.441 722 8	0.603 317 5	−5.871 954 0	1.702 977 5	1.899 345 1
C_{08}	1.709 471 6	0.610 776 4	−0.241 929 3	0.972 874 8	2.676 727 6
C_{70}	0.777 089 2	0.386 196 7	0.026 547 9	−0.229 236 0	1.392 870 3
C_{80}	0.187 546 1	0.173 661 7	0.450 199 5	0.215 043 3	0.361 440 2
α/rad^{-1}	1.122 187 0	1.268 093 4	1.959 014 1	3.567 832 8	0.614 908 3
γ	−0.003 305 5	−0.017 604 5	0.050 152 3	−0.106 144 5	0.014 322 4
rms deviation/cm^{-1}	3.7	23.3	26.2	30.1	9.3

optimized geometries, computed vibrational frequencies, and relative electronic energies are included in the following subsections for the sake of completeness. Nevertheless, we have neither calculated FC factors involving, nor simulated the ionization processes to, these two cationic states (see also later text).

Optimized geometrical parameters and computed vibrational frequencies

Regarding the computed geometrical parameters obtained in the present study for the electronic states considered of SF_2 and its cation, the largest differences of the computed values of the bond lengths r_e(SF) and bond angles θ_e(FSF) obtained using the three different basis sets of valence quadruple-zeta, valence quintuple-zeta, and core-valence quadruple-zeta qualities are <0.005 Å and $<0.7°$, respectively (Tables III and IV). The small ranges of these computed values show that a very high degree of consistency has been achieved. In general, a larger or better quality basis set gives a slightly smaller r_e and a slightly larger θ_e, except for the $\tilde{D}\,^2A_1$ state of SF_2^+, where a better quality basis set gives smaller values of both r_e and θ_e (see Table IV). In all cases, both effects of core correlation and basis size (from quadruple-zeta to quintuple-zeta quality) on the computed geometrical parameters are in the same directions, and in almost all cases, core correlation effects are slightly larger than basis size effects.

There are no experimental geometrical parameters available for any cationic states of SF_2^+ for comparison with our results (Table IV). The computed minimum-energy geometrical parameters reported here are currently the most reliable for these cationic states. For the $\tilde{X}\,^1A_1$ state of SF_2, some previous experimental and calculated geometrical parameters are available (Table III). It is clear from Table III that the calculations performed in the present study are of significantly higher levels than those of previous calculations. Consequently, previous theoretical results are ignored in the following discussion. The most reliable experimental geometrical parameters of the $\tilde{X}\,^1A_1$ state of SF_2 are from the microwave study of Ref. 3. The best theoretical values of r_e and θ_e obtained in the present study, assuming that core correlation and basis set extension effects on the computed geometrical parameters are additive (core+CBS; Table III), are 1.585 ± 0.005 Å and $98.02° \pm 0.06°$, respectively. The uncer-

TABLE III. Computed minimum-energy geometrical parameters (in Å and deg) and vibrational frequencies (fundamental frequencies in parentheses; cm^{-1}) of the $\tilde{X}\,^1A_1$ state of SF_2 obtained at different levels of calculation.

Methods	r(SF)	θ(FSF)	$\omega_1(a_1)$	$\omega_2(a_1)$	$\omega_3(b2)$	Ref.
CCSD(T)/AVQZ[a]	1.592 4	97.94	850.0	356.8	823.9	Present
CCSD(T)/AV5Z[b]	1.589 8	97.96	852.7 (846.6)	358.4 (357.0)		Present
CCSD(T)/ACVQZ[c]	1.588 4	97.99				Present
(Core+CBS)[d]	1.585±0.005	98.02 ±0.06				Present
CISD/6-31G* (Ryd)	1.621	99.02	938 (844)[e]	380 (342)[e]	923 (831)[e]	16
MRDCI/DZ+P	1.599	98.85	(850)	(360)	(819)	13
CASPT2/ANO	1.595	97.4				15
Microwave	1.589	98.3				2
Chemiluminescence	1.592 08	981.97		357±2		4
Microwave	1.587 45 ±0.000 12	98.048 ±0.013				3
IR gas			(838.53)		(813.04)	5
Chemiluminescence			(838±2)	(355±2)	(817±6)	6

[a]The aug-cc-pV(Q+d)Z basis set was used for S and the aug-cc-pVQZ basis set was used for F.
[b]The aug-cc-pV(5+d)Z basis set was used for S and the aug-cc-pV5Z basis set was used for F.
[c]The aug-cc-pwCVQZ basis set was used for S and the aug-cc-pCVQZ basis set was used for F.
[d]Core contributions take the differences between values obtained from RCCSD(T) calculations with only the S $1s^2$ electrons frozen using the aug-cc-pwCVQZ/aug-cc-p-CVQZ basis sets (for S/F) and values from RCCSD(T) calculations with the S $1s^22s^22p^6$ and F $1s^2$ electrons frozen using the aug-cc-pV(Q+d)Z/aug-cc-pVQZ basis sets. Contributions from basis set extension to the complete basis set (CBS) limit take half of the differences between the values obtained using the valence quadruple-zeta quality and valence quintuple-zeta quality basis sets. The core and CBS contributions are assumed to be additive.
[e]Scaled Hartree-Fock harmonic vibrational frequencies $(0.9)\omega_e$ (see Ref. 16).

tainties quoted here are estimated from the differences between the best theoretical values and the calculated values obtained using the quintuple-zeta quality basis sets. It is pleasing that the best theoretical values reported here agree within the estimated theoretical uncertainties with the most reliable experimental values of 1.587 45±0.000 12 Å and 98.048°±0.013° of Ref. 3.

Considering vibrational frequencies, the only available experimental information for SF_2^+ is from the He I PE spectrum of Ref. 20. The vibrationally resolved first PE band[20] gives a value for the symmetric stretching frequency ν_1' of the $\tilde{X}\,^2B_1$ state of SF_2^+ of 935±40 cm^{-1} (Table IV). The corresponding computed fundamental vibrational frequency obtained from the PEF in the present study is 985.6 cm^{-1}; i.e., the experimental value is smaller than the currently best theoretical value from the present work by 50 cm^{-1}. The discrepancy between theory and experiment is outside the quoted experimental uncertainty of ±40 cm^{-1} by 10 cm^{-1}. Considering the computed harmonic vibrational frequencies (both ω_1 and ω_2; see Table IV) of the $\tilde{X}\,^2B_1$ state of SF_2^+ obtained employing the aug-cc-pV(Q+d)Z/aug-cc-pVQZ (computed numerically) and aug-cc-pV(5+d)Z/aug-cc-pV5Z (computed variationally using the PEF) basis sets, the differences are less than 5 cm^{-1}, which may be taken as the theoretical uncertainty associated with the computed vibrational frequencies. In view of the above considerations and an experimental resolution of 45 meV [362 cm^{-1}; full width at half maximum (FWHM)] quoted in Ref. 20, it is concluded that the agreement between theory and experiment in the symmetric stretching frequency of the $\tilde{X}\,^2B_1$ state of SF_2^+ is probably just within the combined experimental and theoretical uncertainties.

For the $\tilde{X}\,^1A_1$ state of SF_2, available experimental and calculated vibrational frequencies are given in Table III. As mentioned above in the discussion on geometrical parameters, as the levels of calculation carried out in the present study are significantly higher than those of previous calculations, the calculated vibrational frequencies reported here are currently the most reliable theoretical values. Comparison with available experimental values gives discrepancies between theory and experiment of less than 10 cm^{-1} (see Table III).

Vertical and adiabatic ionization energies

The first AIE_e of SF_2 obtained in the present study has a best theoretical value of 10.051±0.009 eV (Table V). This value has included contributions from core electron correlation, basis set extension (to the CBS limit), and relativistic effects (see Table V). While contributions from both core electron correlation and basis set extension increase the computed AIE_e value slightly, the relativistic contribution decreases it slightly. The core correlation contribution is small (+0.003 eV), but the relativistic contribution of −0.009 eV is of a similar magnitude to the basis set extension contribution of +0.010 eV. The maximum theoretical uncertainty associated with the best AIE_e value has been estimated based on the difference between the (CBS+core) value (Table V) and the calculated RCCSD(T) value using the valence quintuple-

TABLE IV. Computed minimum-energy geometrical parameters (in Å and deg) and vibrational frequencies (fundamental frequencies in parentheses; cm^{-1}) of some low-lying states of SF_2^+ obtained at different levels of calculation.

	r(SF)	θ(FSF)	$\omega_1(a_1)$	$\omega_2(a_1)$	$\omega_3(b_2)$
		$\tilde{X}\,^2B_1\ (3b_1)^1$			
RCCSD(T)/aug-cc-pVQZ[a]	1.5065	101.64	989.1	411.4	1012.5
RCCSD(T)/aug-cc-pV5Z[b]	1.5039	101.67	992.4 (985.6)	414.8 (413.4)	
RCCSD(T)/aug-cc-pwCVQZ[c]	1.5022	101.72			
He I photoelectron[d]			935±40		
		$\tilde{A}\,^2A_1\ (9a_1)^1(3b_1)^0$			
RCCSD(T)/aug-cc-pVQZ	1.5565	165.56			
RCCSD(T)/aug-cc-pV5Z	1.5532	165.74	705.2 (704.4)	477.5[e]	
RCCSD(T)/aug-cc-pwCVQZ	1.5517	166.25			
		$\tilde{B}\,^2B_2\ (3b_1)^0(6b_2)^1$			
RCCSD(T)/aug-cc-pVQZ	1.5646	85.98			
RCCSD(T)/aug-cc-pV5Z	1.5163	86.05	865.5 (838.2)	562. (557.0)	
RCCSD(T)/aug-cc-pwCVQZ	1.5599	86.09			
		$\tilde{C}\,^2B_2\ (5b_2)^1$			
RCCSD(T)/aug-cc-pVQZ	1.6842	70.27			
RCCSD(T)/aug-cc-pV5Z	1.6816	70.33	785.8 (776.3)	424.1 (416.1)	
RCCSD(T)/aug-cc-pwCVQZ	1.6800	70.39			
		$\tilde{D}\,^2A_1\ (8a_1)^1$			
RCCSD(T)/aug-cc-pVQZ	1.5644	116.03			
RCCSD(T)/aug-cc-pV5Z	1.5610	115.99	718.5 (709.8)	267.9 (265.1)	
RCCSD(T)/aug-cc-pwCVQZ	1.5613	115.88			
		$\tilde{E}\,^2A_2\ (1a_2)^1$			
RCCSD(T)/aug-cc-pVQZ	1.7088	86.75			
RCCSD(T)/aug-cc-pV5Z	1.7062	86.77	712.3 (706.2)	288.3 (285.9)	
RCCSD(T)/aug-cc-pwCVQZ	1.7046	86.81			

[a]The aug-cc-pV(Q+*d*)Z basis set was used for S and the aug-cc-pVQZ basis set was used for F; same below.
[b]The aug-cc-pV(5+*d*)Z basis set was used for S and the aug-cc-pV5Z basis set was used for F; same below.
[c]The aug-cc-pwCVQZ basis set was used for S and the aug-cc-pCVQZ basis set was used for F; same below.
[d]Reference 20.
[e]The bending mode is very anharmonic and the computed fundamental frequency is very dependent on the harmonic basis set used in the vibrational calculation.

zeta quality basis set, plus an estimated uncertainty of 0.001 eV associated with the relativistic contribution (10% of the relativistic contribution). Including ΔZPE as discussed (see also footnote g of Table V), the first AIE_0 of SF_2 has a best theoretical value of 10.075±0.011 eV (the quoted uncertainty has included an estimated uncertainty associated with ΔZPE of 0.002 eV, which is 10% of the ΔZPE value). Regarding the computed AIE_e values for ionizations leading to the excited cationic states of SF_2^+ considered, contributions from core correlation and basis set extension effects behave in a similar way as for the first AIE_e as discussed. The only exception is for the ionization leading to the $\tilde{D}\,^2A_1$ state of SF_2^+, where the core correlation contribution (+0.031 eV) is larger than the basis set extension contribution (+0.023 eV; Table V). In general, contributions from core correlation, basis set extension and relativistic effects to the computed AIE_e values of ionizations leading to the excited cationic states of SF_2^+ considered are significantly larger than those for AIE_e to the $\tilde{X}\,^2B_1$ state of SF_2^+. In addition, the computed relativistic contribution increases the computed AIE_e value to the $\tilde{D}\,^2A_1$ state of SF_2^+ state, in contrast to opposite, decreasing effects for all other cationic states.

As mentioned in the Introduction, the first AIE of SF_2 has been obtained experimentally and computationally on a number of occasions (Table V). The best theoretical value of 10.075±0.011 eV reported here agrees very well with the experimental value of 10.08 eV from the He I PE (Ref. 20) and photoionization mass-spectrometric[19] studies. However, the value of 10.29±0.10 eV, obtained from electron-impact mass-spectrometric studies,[17,18] appears to be too large. Nevertheless, the uncertainty of 0.10 eV quoted in these two-electron-impact studies[17,18] is also quite large. On the other hand, the AIE_0 value of 10.021±0.001 eV deduced in the REMPI study[7] appears to be too small when compared with the best theoretical value obtained here. The REMPI value was obtained from a fit to the Rydberg formula of the $ns(\tilde{B}\,^1B_1)$ $(n=4,5)$ origins with values of 54 433 and 68 951 cm^{-1} (6.75 and 8.55 eV, respectively; see footnote h of Table V and the original work[7]). The energy positions of

TABLE V. Computed adiabatic (AIE) and vertical (VIE) ionization energies (in eV) of some lo-lying cationic states of SF_2^+ obtained at different levels of calculation.

State open-shell configuration	AIE		VIE		Ref.
$\tilde{X}\,^2B_1\ (3b_1)^1$	RCCSD	RCCSD(T)	RCCSD	RCCSD(T)	
aug-cc-pV(Q+*d*)Z[a]	10.027	10.042	10.391	10.336	Present
aug-ccpV(5+*d*)Z[b]	10.034	10.052	10.400	10.348	Present
aug-cc-pwCVQZ[c]	10.025	10.045	10.397	10.342	Present
(CBS+core)[d]		10.060±0.008		10.36±0.01	Present
Relativistic[e]		−0.009			Present
Best theoretical AIE_e[f]		10.051±0.009			Present
AIE_0 (AIE_e+ΔZPE[g])		10.075±0.011			Present
G2		10.15			21 and 22
CCSD(T)/cc-pVTZ				10.28	40
Mass spect. (e-impact)		10.29±0.10			17
He I photoelectron		10.08		10.31	20
Mass spect. (e-impact)		10.29±0.10			18
Mass spect. (photoion.)		10.08			19
REMPI (Rydberg series)[h]		10.021(1)			7
$\tilde{A}\,^2A_1\ (3b_1)^0(9a_1)^1$					
aug-cc-pV(Q+*d*)Z	13.135	12.875	15.884	15.536	Present
aug-cc-pV(5+*d*)Z	13.154	12.894	15.909	15.563	Present
aug-cc-pwCVQZ	13.138	12.875	15.904	15.557	Present
(CBS+core)		12.91±0.02		15.60±0.03	Present
Relativistic		−0.030			Present
Best theoretical AIE_e		12.87±0.02			Present
AIE_0 (AIE_e+ΔZPE[g])		12.87±0.03			Present
$\tilde{B}\,^2B_2\ (3b_1)^0(6b_2)^1$					
aug-cc-pV(Q+*d*)Z	14.151	13.986	14.611	14.384	Present
aug-cc-pV(5+*d*)Z	14.164	14.003	14.626	14.403	Present
aug-cc-pwCVQZ	14.165	14.001	14.629	14.400	Present
(CBS+core)		14.03±0.02		14.43±0.03	Present
Relativistic		−0.020			Present
Best theoretical AIE_e		14.01±0.02			Present
AIE_0 (AIE_e+ΔZPE[g])		14.00±0.03			Present
$\tilde{C}\,^2B_2(5b_2)^1$					
aug-cc-pV(Q+*d*)Z	15.314	15.179	16.261	16.112	Present
aug-cc-pV(5+*d*)Z	15.354	15.220	16.305	16.156	Present
aug-cc-pwCVQZ	15.347	15.207	16.294	16.140	Present
(CBS+core)		15.27±0.05		16.21±0.05	Present
Relativistic		−0.032			Present
Best theoretical AIE_e		15.24±0.05			Present
AIE_0 (AIE_e+ΔZPE[g])		15.21±0.06			Present
He I photoelectron				(16.20)	20
$\tilde{D}^2A_1\ (8a_1)^1$					
aug-cc-pV(Q+*d*)Z	15.406	15.278	15.632	15.492	Present
aug-cc-pV(5+*d*)Z	15.428	15.301	15.657	15.517	Present
aug-cc-pwCVQZ	15.438	15.309	15.663	15.520	Present
(CBS+core)		15.34±0.04		15.56±0.04	Present
Relativistic		+0.016			Present
Best theoretical AIE_e		15.36±0.04			Present
AIE_0 (AIE_e+ΔZPE		15.35±0.05			Present
He I photoelectron				15.40	20
$\tilde{E}\,^2A_2\ (1a_2)^1$					
aug-cc-pV(Q+*d*)Z	16.512	16.138	16.896	16.595	Present
aug-cc-pV(5+*d*)Z	16.558	16.183	16.946	16.643	Present
aug-cc-pwCVQZ	16.553	16.170	16.938	16.629	Present
(CBS+core)		16.24±0.05		16.70±0.06	Present
Relativistic		−0.032			Present

TABLE V. (*Continued.*)

State open-shell configuration	AIE	VIE	Ref.
Best theoretical AIE_e	16.21±0.05		Present
AIE_0 ($AIE_e+\Delta ZPE$[g])	16.19±0.06		Present
He I photoelectron		(16.20)	20

[a]The aug-cc-pV(Q+*d*)Z basis set was used for S and the aug-cc-pVQZ basis set was used for F; same below.
[b]The aug-cc-pV(5+*d*)Z basis set was used for S and the aug-cc-pV5Z basis set was used for F; same below.
[c]the aug-cc-pwCVQZ basis set was used for S and the aug-cc-pCVQZ basis set was used for F; same below.
[d]Core contributions take the differences between AIE or VIE values obtained from RCCSD(T) calculations with only the S $1s^2$ electrons frozen using the aug-cc-pwCVQZ/aug-cc-pCVQZ basis sets (for S/F) and values from RCCSD/T calculations with the S $1s^22s^22p^6$ and F $1s^2$ electrons frozen using the aug-cc-pV(Q+*d*)Z/aug-cc-pVQZ basis sets. Contributions from basis set extension to the complete basis set (CBS) limit take half of the difference between the values obtained using the valence quadruple-zeta quality and valence quintuple-zeta quality basis sets. The core and CBS contributions are assumed to be additive (same below).
[e]Relativistic contributions using two methods give almost identical results. Hence only one value is given for the sake of simplicity (same below).
[f]The best theoretical AIE_e values include core, CBS, and relativistic contributions (same below).
[g]Zero-point energy corrections (ΔZPE) have been evaluated employing the computed vibrational frequencies given in Table II. For the ionization to the $\tilde{X}\,^2B_1$ state of SF_2^+, the harmonic vibrational frequencies of all three modes obtained at the RCCSD(T)/aug-cc-pVQZ level were used. For other higher IE ionizations, the calculated fundamental vibrational frequencies of the symmetric stretching and bending modes obtained from the RCCSD(T)/aug-cc-pV5Z PEFs were used.
[h]The AIE_0 value was obtained from a fit to the Rydberg formula of the $ns(\tilde{B}\,^1B_1)$ (n=4, 5) origins. The $\tilde{B}\,^1B_1(4s)$ and $\tilde{B}\,^1B_1(5s)$ origins from Ref. 7 are 54 470 and 68 951 cm−1, but the former value was obtained by extrapolation (see original work). The authors of Ref. 7 believe that a value of 54 433 cm^{-1} from an earlier REMPI study (Ref. 41) for the $\tilde{B}\,^1B_1(4s)$ origin is more accurate and may have used the earlier value in their fit to obtain the AIE_0.

the origins of these two Rydberg states are still quite far away from the first ionization limit of ca. 10 eV and may be perturbed by interaction with other states. The uncertainty associated with the first AIE_0 value derived in the REMPI study[7] is probably larger than the quoted uncertainty of 0.001 eV.

For the higher IE bands of SF_2 in the observed He I PE spectrum,[20] no AIE position is identifiable because of overlapping bands as mentioned in the Introduction (see also Fig. 2). Nevertheless, the spectral features observed at 15.40, 16.20, 18.3, and 19.3 eV of the He I PE spectrum[20] have been assigned to the VIE positions of the $(8a_1)^{-1}$, $\{(5b_2)^{-1}$ and $(1a_2)^{-1}\}$, $(2b_1)^{-1}$, and $(7a_1)^{-1}$ ionizations of SF_2 based on computed VIEs as discussed in the Introduction (see Table VI and its footnotes). The computed and experimental VIE values from Ref. 20 are compared with the computed VIE values obtained here in Table VI (see also Table V). In general, our *ab initio* VIE values support the assignments of the ionization processes made in Ref. 20. In fact, the agreement of our calculated VIE values with the experimental values is much better than that of the lower-level calculations of Ref. 20. However, the true VIE position of a PE band depends on the FC factors between the two states involved, which will be considered in the next subsection on spectral simulations.

TABLE VI. Computed vertical (VIE) ionization energies (in eV) of some low-lying cationic states of SF_2^+ obtained at different levels of calculation using the aug-cc-pV(Q+*d*)Z (aug-cc-pVQZ basis sets for S (F) at the RCCSD(T) minimum-energy geometry of the $\tilde{X}\,^1A_1$ state of SF_2 using the same basis set.

State, configuration	CAS	MRCI	MRCI+D	RCCSD	RCCSD(T)	He I[a]	HFS[b]	KT[c]
$^2B_1\ (3b_1)^1$	9.29	9.99	10.12	10.39	10.34	10.31	9.77	9.68
$^2B_2\ (3b_1)^0(6b_2)^1$	13.97	14.26	14.25	14.61	14.38	[d]		
$^2A_1\ (8a_1)^1$	14.59	15.09	15.14	15.63	15.49	15.4	14.68	14.29
$^2A_1\ (9a_1)^1(3b_1)^0$	15.24	15.59	15.61	15.88	15.54	[d]		
$^2B_2\ (5b_2)^1$	15.09	15.78	15.90	16.26	16.14	16.2	15.56	15.61
$^2A_2\ (1a_2)^1$	15.51	16.21	16.31	16.90	16.60	16.2	15.52	16.44
$^2B_1\ (2b_1)^1(3b_1)^2$	16.79	17.49	17.57			18.3	16.55	17.47
$^2A_2\ (8a_1)^1(3b_1)^1(6b_2)^1$	18.06	18.64	18.65			[d]		

[a]Experimental values from He I photoelectron spectrum of Ref. 20; note that the b_1 and b_2 irreducible representations of the C_{2v} symmetry point group used in Ref. 20 correspond to b_2 and b_1 used here because of the different molecular axes used. Also, the molecular orbital numbering in Ref. 20 considers only valence electrons, but we have considered all electrons, including the core electrons.
[b]From HFS-$X\alpha$ (transition state) calculation of Ref. 20.
[c]Scaled Koopmann's theorem values [0.92 × (negative orbital energies)] of HF calculation of Ref. 23 (see also Ref. 20).
[d]These states cannot be reached by one-electron ionizations and hence are forbidden.

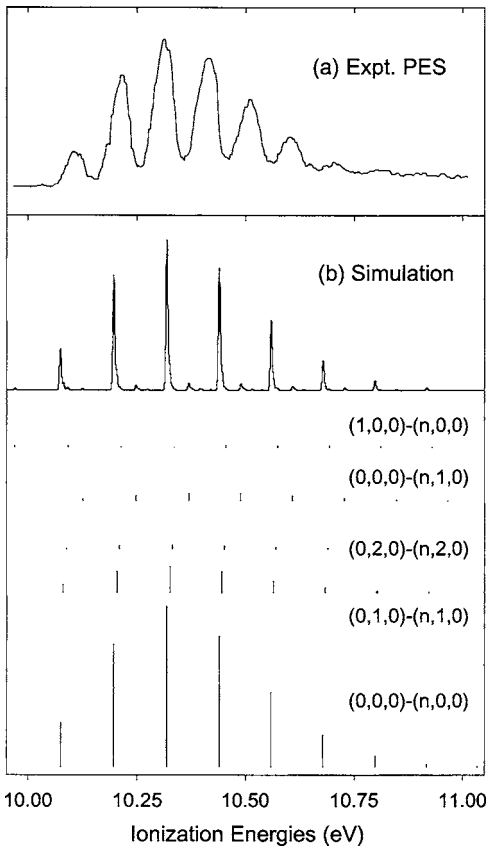

FIG. 1. (a) The first band ($SF_2^+\tilde{X}\,^2B_1 \leftarrow SF_2\tilde{X}\,^1A_1$) in the experimental He I photoelectron spectrum of SF_2 (Ref. 20) and (b) the corresponding simulated spectrum employing the geometries of the $\tilde{X}\,^1A_1$ state of SF_2 and the $\tilde{X}\,^2B_1$ states of SF_2^+ obtained from the *ab initio* potential energy functions, the best theoretical AIE_0 (see Table V) value, a Boltzmann distribution of the low-lying vibrational levels of $\tilde{X}\,^1A_1$ state of SF_2 with a vibrational temperature of 300 K, and a FWHM of 5 meV for each vibrational component; the bar diagrams underneath the simulated spectrum show the computed FCFs and vibrational designations of the major vibrational progressions contributing to the PE band.

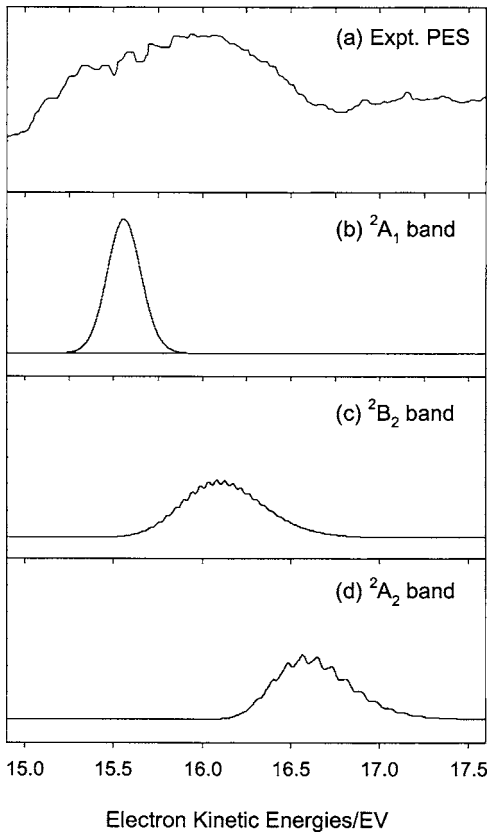

FIG. 2. (a) The experimental He I photoelectron spectrum of SF_2 in the 15–17 eV region (Ref. 20) and the simulated ionization from the $\tilde{X}\,^1A_1$ state of SF_2 to the (b) $\tilde{D}\,^2A_1$, (c) $\tilde{C}\,^2B_2$, and (d) $\tilde{E}\,^2A_2$ states of SF_2^+, a FWHM of 45 meV for each vibrational component has been used in the simulated spectra.

The one-electron forbidden $\tilde{A}\,^2A_1$ and $\tilde{B}\,^2B_2$ states of SF_2^+

Before the various simulated bands of the PE spectrum of SF_2 are discussed, the one-electron forbidden $\tilde{A}\,^2A_1$ and $\tilde{B}\,^2B_2$ states of SF_2^+ are further considered. For the $\tilde{B}\,^2B_2$ state, the computed AIE_e (14.01 eV) and VIE_e (14.43 eV) are lower than those of the one-electron allowed $\tilde{C}\,^2B_2$ state (15.24 and 16.21 eV; respectively Table V) by 1.23 and 1.78 eV, respectively, indicating that the electronic energy surfaces of these two states are quite apart in energy from each other in the region relevant to the PE spectrum of SF_2. In addition, the computed electronic wave functions of the $\tilde{B}\,^2B_2$ and $\tilde{C}\,^2B_2$ states of SF_2^+ obtained from the two-state CASSCF/MRCI calculations at the minimum-energy geometry of the $\tilde{X}\,^1A_1$ state of SF_2 give computed coefficients of the leading electronic configurations larger than 0.9 for both states, showing that there is negligible mixing between these two $^2B_2$ states through configuration interaction (CI) in the VIE region. Therefore, it is safely concluded that the one-electron forbidden ionization process to the $\tilde{B}\,^2B_2$ state of SF_2^+ can be ignored in the consideration of the He I PE spectrum of SF_2.

However, regarding the $\tilde{A}\,^2A_1$ state, the best computed VIE (15.60 eV) is very slightly higher than that of the $\tilde{D}\,^2A_1$ state (15.56 eV), suggesting that the electronic surfaces of these two states should intersect near the VIE region and would interact via CI at the intersections. From the results of energy scans carried out in the present study, these two $^2A_1$ surfaces intersect in a region with ca. θ=94° (and r with values of ca. 1.5 Å). At regions with θ smaller than 93°, the $\tilde{A}\,^2A_1$ surface is above the $\tilde{D}\,^2A_1$ surface. The computed CASSCF and MRCI wave functions of the $\tilde{A}\,^2A_1$ and $\tilde{D}\,^2A_1$ states of SF_2^+ at the minimum-energy geometry of the $\tilde{X}\,^1A_1$ state of SF_2 (i.e., at the VIE region) obtained from the two-state CASSCF/MRCI calculations suggest strong CI mixing between these two $^2A_1$ states. However, RCCSD(T) calculations on these two $^2A_1$ states at the VIE region give T_1 diagnostic values of less than 0.029 for both states, suggesting negligible multireference character. Single-state CASSCF/MRCI calculations on the $\tilde{D}\,^2A_1$ state at the minimum-energy geometry of the $\tilde{X}\,^1A_1$ state of SF_2 (the $\tilde{D}\,^2A_1$ state is slightly lower in energy than the $\tilde{A}\,^2A_1$ state at this geometry) give CASSCF and MRCI wave functions with only one major configuration of the $\tilde{D}\,^2A_1$ state (computed CI coefficients

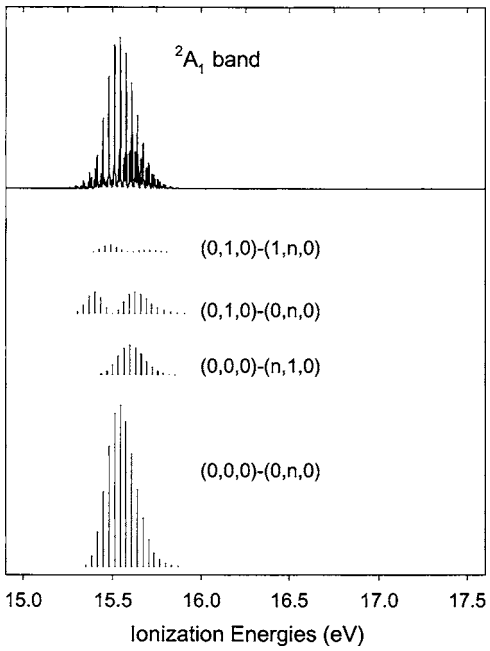

FIG. 3. The simulated spectrum of the $SF_2^+\tilde{D}\,^2A_1 \leftarrow SF_2\tilde{X}\,^1A_1$ ionization employing the corresponding geometries obtained from the *ab initio* potential energy functions, the best theoretical AIE_0 (see Table V) value, a Boltzmann distribution for the low-lying vibrational levels of $\tilde{X}\,^1A_1$ state of SF_2 with a vibrational temperature of 300 K, and a FWHM of 5 meV for each vibrational component; the bar diagrams underneath the simulated spectrum show the computed FCFs and vibrational designations of the major vibrational progressions contributing to the PE band.

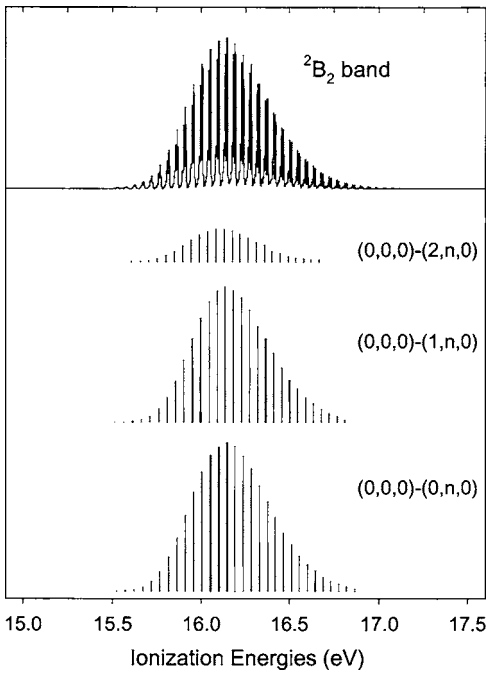

FIG. 4. The simulated spectrum of the $SF_2^+\tilde{C}\,^2B_2 \leftarrow SF_2\tilde{X}\,^1A_1$ ionization employing the corresponding geometries obtained from the *ab initio* potential energy functions, the best theoretical AIE_0 (see Table V) value, a Boltzmann distribution for the low-lying vibrational levels of the $\tilde{X}\,^1A_1$ state of SF_2 with a vibrational temperature of 300 K, and a FWHM of 5 meV for each vibrational component; the bar diagrams underneath the simulated spectrum show the computed FCFs and vibrational designations of the major vibrational progressions contributing to the PE band.

are 0.958 and 0.915 in the CASSCF and MRCI calculations, respectively), with very little CI mixing from the $\tilde{A}\,^2A_1$ state (computed CI coefficients are smaller than 0.05). These results from RCCSD(T) and single-state CASSCF/MRCI calculations suggest that the computed strong CI mixing between the two $^2A_1$ states in the two-state average-state CASSCF/MRCI calculations could very likely be an artifact resulting from the averaged-state CASSCF molecular orbitals, which are not optimal for both $^2A_1$ states and hence give poor descriptions for each of the two states at this geometry in the VIE region. Consequently, significant CI mixings arise in order to compensate for the poor (for each state) many-particle basis used in the CASSCF/MRCI calculations. Computed restricted-spin Hartree-Fock (RHF) wave functions of the $\tilde{A}\,^2A_1$ and $\tilde{D}\,^2A_1$ states in the VIE region show that their molecular orbitals differ significantly, as expected. For example, the $(8a_1)^2$ molecular orbital of the $\tilde{A}\,^2A_1$ state has negligible contribution from F $2p_y$ basis functions (the yz plane is the molecular plane and the z axis is the C_2 axis), while the $(8a_1)^1$ molecular orbital of the $\tilde{D}\,^2A_1$ state has a nontrivial contribution from F $2p_y$ basis functions. The computed charge densities according to the Mulliken population analysis on the RHF wave functions of the $\tilde{A}\,^2A_1$ and $\tilde{D}\,^2A_1$ states are {S(+1.685);F(−0.342)} and {S(+1.479); F(−0.239)}, respectively, which also show that the electron distributions as obtained from the RHF wave functions of the two $^2A_1$ states are quite different. Summarizing, the electronic energy surfaces of the $\tilde{A}\,^2A_1$ and $\tilde{D}\,^2A_1$ states of SF_2^+ intersect near the VIE region and would interact via CI. However, the strong computed CI mixings between the two surfaces from the two-state average-state CASSCF/MRCI calculations may have been exaggerated, because of the use of the average-state many-particle basis. Although we have not considered the ionization process to the one-electron forbidden $\tilde{A}\,^2A_1$ state in the following spectral simulations, it should be noted that the ionization process to the one-electron allowed $\tilde{D}\,^2A_1$ state could be perturbed by the $\tilde{A}\,^2A_1$ state near the region where the electronic surfaces of these two $^2A_1$ states cross each other.

Spectral simulations: First PE band of SF_2

The observed first PE band of SF_2 in the He I spectrum of Ref. 20 and the corresponding simulated spectrum obtained in the present investigation are shown in Figs. 1(a) and 1(b), respectively. In the spectral simulation, the geometries, as obtained from the respective *ab initio* PEFs of the two states involved, and the best theoretical AIE_0 value of 10.075 eV (Table V) were employed. A Boltzmann distribution with a vibrational temperature of 300 K has been assumed for the populations of the low-lying vibrational levels of the $\tilde{X}\,^1A_1$ state of SF_2. A Gaussian function with a FWHM of 5 meV was used for each vibrational component in Fig. 1(b). Such a small FWHM was used in order to show the weak vibrational structure (or "hot bands") arising from ionization from excited vibrational levels of the $\tilde{X}\,^1A_1$ state of SF_2. The computed Franck-Condon Factors (FCFs) of the major vibrational progressions involved, including those of

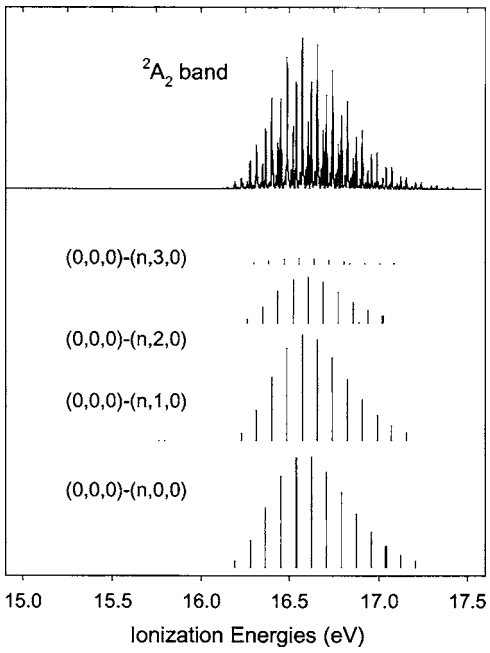

FIG. 5. The simulated spectrum of the $SF_2^+\tilde{E}\,^2A_2 \leftarrow SF_2\tilde{X}\,^1A_1$ ionization employing the corresponding geometries obtained from the *ab initio* potential energy functions, the best theoretical AIE_0 (see Table V) value, a Boltzmann distribution for the low-lying vibrational levels of the $\tilde{X}\,^1A_1$ state of SF_2 with a vibrational temperature of 300 K, and a FWHM of 5 meV for each vibrational component; the bar diagrams underneath the simulated spectrum show the computed FCFs and vibrational designations of the major vibrational progressions contributing to the PE band.

the hot bands (and their vibrational designations), are shown underneath the simulated spectrum of Fig. 1(b). It is pleasing to see that the relative intensities of the vibrational components in the simulated first PE band of SF_2 [Fig. 1(b)] agree very well with those of the observed spectrum [Fig. 1(a)]. It is therefore concluded that the computed geometry change upon ionization is close to the true one, and the assumption of a Boltzmann distribution with a vibrational temperature of 300 K for the populations of low-lying vibrational levels of the $\tilde{X}\,^1A_1$ state of SF_2 is reasonable. With the best *ab initio* AIE_0 value of 10.075 eV, a VIE value of 10.319 eV is obtained from the simulated first PE band of SF_2, which is the position of the $SF_2^+\tilde{X}\,^2B_1(2,0,0) \leftarrow SF_2\tilde{X}\,^1A_1(0,0,0)$ vibrational component (see Fig. 1). This VIE value obtained form the FCF calculations agrees very well with the experimental VIE value of 10.31 eV from Ref. 20.

However, from Fig. 1, it can be seen that the simulated and experimental spectra are not identical. Specifically, the position of the first vibrational component does not match between the simulated and observed spectra. In addition, vibrational spacings in the simulated PE band [Fig. 1(b)] are significantly larger than those in the observed band [Fig. 1(b)]. It has been discussed above that the computed fundamental vibrational frequency of the symmetric stretching mode of the $\tilde{X}\,^2B_1$ state of SF_2^+ is larger than the observed value of Ref. 20 by 50 cm^{-1}. However, this relatively small difference between the computed and observed vibrational frequencies cannot lead to such a large difference between the simulated and observed spectra as shown in Fig. 1. Based on the energy scale given in Fig. 2 of Ref. 20 [as shown in Fig. 1(a) here], the averaged experimental vibrational spacing is estimated to be only ca. 810 cm^{-1} (with an estimated uncertainty of ca. 40 cm^{-1}), which is significantly smaller than the value of 935 ± 40 cm^{-1} given in the text of Ref. 20. In addition, the position of the first vibrational component as shown in the experimental spectrum of Fig. 1(a) is estimated to be 10.11 eV, which is significantly larger than the value of 10.08 eV given in Table I of Ref. 20. These inconsistencies in the AIE_0 and vibrational spacings between values from the figure and the text/table of Ref. 20 and also the poor agreement between the simulated and observed first PE bands of SF_2 as shown in Fig. 1 here suggest that the energy scale given in the published experimental first band of SF_2 is almost certainly unreliable. It should be noted that in Ref. 20, known IEs of N_2 were used for energy calibration. The first AIE of N_2 has a value of ca. 15.6 eV, which is over 5 eV higher than that of the first PE band of SF_2. In view of the above considerations, it is concluded that the energy scale used in the published figure of the first PE band of SF_2 from Ref. 20 is probably unreliable and further experimental investigations are called for. Nevertheless, the experimental AIE, VIE, and symmetric stretching vibrational frequency given in the text and table of Ref. 20 for the first PE band of SF_2 appear to be reasonably reliable when compared with the corresponding *ab initio* values obtained in the present study. Also, the excellent agreement between simulated and observed relative intensities of the vibrational components of the first PE band of SF_2 supports the assignments of the molecular species, electronic states involved, and the vibrational structure given in Ref. 20.

Spectral simulations: Higher IE bands of SF_2

The simulations of the bands corresponding to ionizations to the one-electron allowed $\tilde{C}\,^2B_2$, $\tilde{D}\,^2A_1$, and $\tilde{E}\,^2A_2$ states of SF_2^+ from the $\tilde{X}\,^1A_1$ state of SF_2 are given in Fig. 2, and also individually in Figs. 3–5, respectively, together with the corresponding computed FCFs of the major vibrational progressions and their designations. In Fig. 2, simulated bands have a FWHM of 45 meV for each vibrational component, which is the quoted resolution of the experimental He I spectrum of Ref. 20. However, in Figs. 3–5, a much smaller FWHM of 5 meV has been used in order to show the complex and overlapping vibrational structure in each band. Similar to the simulation of the first PE band of SF_2 discussed above, *ab initio* geometries from the PEFs, the best *ab initio* AIE_0 values, and a Boltzmann distribution with a vibrational temperature of 300 K have been used in the simulation of the higher IE $\tilde{C}\,^2B_2$, $\tilde{D}\,^2A_1$, and $\tilde{E}\,^2A_2$ PE bands.

First, it should be noted that although the $\tilde{C}\,^2B_2$ PE band has a lower computed AIE than the $\tilde{D}\,^2A_1$ PE band (Table V), the computed VIE of the $\tilde{D}\,^2A_1$ PE band is lower than that of the $\tilde{C}\,^2B_2$ PE band (Tables V and VI). In addition, vibrational components in the AIE region of the $\tilde{C}\,^2B_2$ PE band have very low computed FCFs, because of the large changes in geometrical parameters (ca. +0.09 Å and −27.6°;

see Tables III and IV, Fig. 4, and later text) upon ionization. Consequently, the simulated $\tilde{D}\,^2A_1$ PE band appears at a lower IE than the simulated $\tilde{C}\,^2B_2$ PE band, as shown in Fig. 2.

Second, it is not possible to make any detailed comparison between the simulated spectrum of SF_2 in the higher IE region and the observed spectrum in the same IE region as shown in Fig. 2, simply because the observed spectrum consists of too many overlapping bands from other species. Nevertheless, from the computed FCFs and the simulated spectra (Figs. 3–5), the VIE positions of the $\tilde{C}\,^2B_2$, $\tilde{D}\,^2A_1$, and $\tilde{E}\,^2A_2$ PE bands are at 16.15, 15.56, and 16.58 eV. When these values are compared with the experimental values of 16.2, 15.4, and 16.2 eV given in Ref. 20, the agreement is reasonably good for the $\tilde{C}\,^2B_2$ and $\tilde{D}\,^2A_1$ PE bands. However, our calculations and spectral simulations suggest that the VIE position of the $\tilde{E}\,^2A_2$ PE band is higher than 16.2 eV and has not been identified in the He I PE spectrum reported in Ref. 20.

Third, for the $\tilde{D}\,^2A_1$ and $\tilde{E}\,^2A_2$ PE bands, the VIE positions correspond to the $\tilde{D}\,^2A_1(0,6,0)\leftarrow\tilde{X}\,^1A_1(0,0,0)$ and $\tilde{E}\,^2A_2(4,1,0)\leftarrow\tilde{X}\,^1A_1(0,0,0)$ vibrational components, respectively (see Figs. 3 and 5). For the $\tilde{C}\,^2B_2$ PE band, the strongest vibration progression has been assigned to the $\tilde{C}\,^2B_2(0,v_2',0)\leftarrow\tilde{X}\,^1A_1(0,0,0)$ progression (see Fig. 4). However, the computed anharmonic vibrational wave functions of the $\tilde{C}\,^2B_2(0,v_2',0)$ state of SF_2^+ show strong mixings of harmonic functions of the types $h(0,v_2',0)$ and $h(v_1',v_2',0)$, even for low-lying vibrational levels. Nevertheless, the designation of $(0,v_2',0)$ can be confidently made based on the computed coefficients of the harmonic functions in the anharmonic vibrational wave functions for the lowest three vibrational levels of the series and inspections of the nodal characters of the computed anharmonic vibrational wave functions of levels with v_2' of up to 13. For higher vibrational levels, v_2' is no longer a good quantum number for this vibrational progression. The strongest vibrational component of this dominant progression in the $\tilde{C}\,^2B_2$ PE band is the 19th component of the series. Assuming that v_2' is still a good quantum number, the strongest vibrational component of this series may be designated as $\tilde{C}\,^2B_2(0,18,0)\leftarrow\tilde{X}\,^1A_1(0,0,0)$.

CONCLUSION

State-of-the-art *ab initio* calculations have been carried out on the $\tilde{X}\,^1A_1$ state of SF_2 and the $\tilde{X}\,^2B_1$, $\tilde{A}\,^2A_1$, $\tilde{B}\,^2B_2$, $\tilde{C}\,^2B_2$, $\tilde{D}\,^2A_1$, and $\tilde{E}\,^2A_2$ states of SF_2^+. RCCSD(T) potential energy functions of all these neutral and cationic states have been calculated employing basis sets of quintuple-zeta quality. Minimum-energy geometrical parameters and vibrational frequencies have been computed and they compare very well with available experimental results. Reliable adiabatic and vertical ionization energies have been calculated for ionization processes leading to low-lying cationic states of SF_2^+. Based on the best theoretical first AIE_0 value, the reliability of previously reported experimental values has been assessed.

Franck-Condon factors including Duschinsky rotation and anharmonicity have been computed for ionizations from the $\tilde{X}\,^1A_1$ state of SF_2 to the one-electron allowed $\tilde{X}\,^2B_1$, $\tilde{C}\,^2B_2$, $\tilde{D}\,^2A_1$, and $\tilde{E}\,^2A_2$ states of SF_2^+ and photoelectron bands for these ionizations have been simulated. Comparison between the pure "theoretical" photoelectron spectrum of the $SF_2^+\ \tilde{X}\,^2B_1\leftarrow SF_2\ \tilde{X}\,^1A_1$ ionization with the first band in the experimental He I photoelectron spectrum[20] of SF_2 leads to the following conclusions. First, the excellent agreement between the simulated and observed relative intensities of the vibrational components suggests that the computed *ab initio* geometry changes upon ionization are highly reliable. Second, the energy scale in the figure of the published experimental first PE band of SF_2 from Ref. 20 is unreliable and further experimental investigation, particularly including reliable energy calibration, is called for. Nevertheless, the values of AIE, VIE, and vibrational spacing of the first PE band of SF_2 reported in the table and/or the text of Ref. 20 are reliable.

Although it has not been possible to compare the simulated higher IE bands of SF_2 with the experimental He I spectrum reported in Ref. 20, because of overlapping bands in the latter from other species in the higher IE region, VIE values obtained from FCF calculations and spectral simulations support the assignments of the bands at VIE positions of 15.4 and 16.2 eV in the He I PE spectrum by de Leeuw *et al.*[20] to ionizations from the $\tilde{X}\,^1A_1$ state of SF_2 to the $\tilde{D}\,^2A_1$ and $\tilde{C}\,^2B_2$ states of SF_2^+. However, our FC calculations and spectral simulations suggest that the VIE position of the SF_2^+ $\tilde{E}\,^2A_2\leftarrow SF_2\ \tilde{X}\,^1A_1$ ionization should be at 16.58 eV, a higher IE position than the 16.2 eV assigned by de Leeuw *et al.*[20] Finally, the excellent agreement between the simulated and observed first PE bands of SF_2 suggests that the simulated higher IE bands of SF_2 reported here should be reliable. We hope that the present study would prompt further spectroscopic investigations on low-lying excited cationic states of SF_2^+.

ACKNOWLEDGMENTS

Financial support from the Research Grant Council (RGC) of the Hong Kong Special Administrative Region (HKSAR, Grant Nos. AoE/B-10/1 PolyU and PolyU 5003/04P) and provision of computational resources from the EPSRC (U.K.) National Service for Computational Chemistry Software are acknowledged.

[1] K. L. Baluja and J. A. Tossell, J. Phys. B **37**, 609 (2004).
[2] D. R. Johnson and F. X. Powell, Science **164**, 950 (1969).
[3] Y. Endo, S. Saito, E. Hirota, and T. Chikaraishi, J. Mol. Spectrosc. **77**, 222 (1979).
[4] W. H. Kirchhoff, D. R. John, and F. X. Powell, J. Mol. Spectrosc. **48**, 157 (1973).
[5] J. C. Deroche, H. Burger, P. Schulz, and H. Willner, J. Mol. Spectrosc. **89**, 269 (1981).
[6] R. J. Glinski, C. D. Taylor, and F. W. Kutzler, J. Phys. Chem. **96**, 6196 (1990).
[7] Q. X. Li, J. N. Shu, Q. Zhang, S. Q. Yu, L. M. Zhang, C. X. Chen, and X. X. Ma, J. Phys. Chem. A **102**, 7233 (1998).

[8] Q. X. Li, Q. Zhang, J. N. Shu, S. Q. Yu, Q. H. Song, C. X. Chen, and X. X. Ma, Chem. Phys. Lett. **305**, 79 (1999).
[9] X. G. Zhou, Q. X. Li, Q. Zhang, S. Q. Yu, C. X. Chen, and X. X. Ma, J. Electron Spectrosc. Relat. Phenom. **108**, 135 (2000).
[10] X. G. Zhou, S. Q. Yu, Z. Y. Sheng, X. X. Ma, Y. J. Lui, M. B. Huang, and Q. X. Li, Surf. Rev. Lett. **9**, 69 (2002).
[11] T. Ziegler and G. L. Gutsev, J. Chem. Phys. **96**, 7623 (1992).
[12] R. A. King, J. M. Galbraith, and H. F. Schaefer III, J. Phys. Chem. **100**, 6061 (1996).
[13] Z. L. Cai and J. L. Bai, Chem. Phys. Lett. **220**, 109 (1994).
[14] Y.-J. Liu, M.-B. Huang, X. Zhou, and S. Yu, Chem. Phys. Lett. **345**, 505 (2001).
[15] Y.-J. Liu and M.-B. Huang, Chem. Phys. Lett. **360**, 400 (2002).
[16] H. Yu, J. D. Goddard, and D. J. Clouthier, Chem. Phys. Lett. **178**, 341 (1991).
[17] D. L. Hildenbrand, J. Phys. Chem. **77**, 879 (1973).
[18] W. Gombler, A. Hess, and H. Willner, Z. Anorg. Allg. Chem. **469**, 135 (1980).
[19] O. Losking and H. Willner, Z. Anorg. Allg. Chem. **530**, 169 (1985).
[20] D. M. de Leeuw, R. Mooyman, and C. A. de Lange, Chem. Phys. **34**, 287 (1978).
[21] Y. S. Cheung, Y.-T. Chen, C. Y. Ng, S.-W. Chiu, and W.-K. Li, J. Am. Chem. Soc. **117**, 9725 (1995).
[22] K. K. Irikura, J. Chem. Phys. **102**, 5357 (1995).
[23] C. Thomas, Chem. Phys. Lett. **44**, 475 (1976).
[24] D. W. K. Mok, E. P. F. Lee, F.-T. Chau, D.-C. Wang, and J. M. Dyke, J. Chem. Phys. **113**, 5791 (2000).
[25] F.-T. Chau, J. M. Dyke, E. P. F. Lee, and D. K. W. Mok, J. Chem. Phys. **115**, 5816 (2001).
[26] J. M. Dyke, E. P. F. Lee, D. K. W. Mok, and F.-T. Chau, ChemPhysChem **6**, 2046 (2005).
[27] C. Hampel, K. Peterson, and H.-J. Werner, Chem. Phys. Lett. **190**, 1 (1992).
[28] J. D. Watts, J. Gauss, and R. J. Bartlett, J. Chem. Phys. **98**, 8718 (1993).
[29] T. H. Dunning, Jr., K. A. Peterson, and A. K. Wilson, J. Chem. Phys. **114**, 9244 (2001).
[30] K. A. Peterson and T. H. Dunning, J. Chem. Phys. **117**, 10548 (2002).
[31] E. P. F. Lee, J. M. Dyke, F.-T. Chau, and W.-K. Chow, Chem. Phys. Lett. **376**, 465 (2003).
[32] H. J. Werner, D. J. Knowles, R. D. Amos *et al.*, MOLPRO, a package of *ab initio* programs, Version 2002.1.
[33] D. K. W. Mok, F.-T. Chau, E. P. F. Lee, and J. M. Dyke, ChemPhysChem **6**, 719 (2005).
[34] H.-J. Werner and P. J. Knowles, J. Chem. Phys. **82**, 5053 (1985).
[35] P. J. Knowles and H.-J. Werner, Chem. Phys. Lett. **145**, 514 (1988).
[36] W. Meyer, P. Botschwina, and P. Burton, J. Chem. Phys. **84**, 891 (1986).
[37] S. Carter and N. C. Handy, J. Chem. Phys. **87**, 4294 (1987).
[38] J. E. Dennis, Jr., D. M. Gay, and R. E. Welsh, ACM Trans. Math. Softw. **7**, 348 (1981); ACM Trans. Math. Softw. **7**, 369 (1981).
[39] J. K. G. Watson, Mol. Phys. **19**, 465 (1970).
[40] M. A. Ali, K. K. Irikuraa, and Y.-K. Kim, Int. J. Mass. Spectrom. **201**, 187 (2000).
[41] R. D. Johnson III and J. W. Hudgens, J. Phys. Chem. **94**, 3272 (1990).